Pharmacology Research & Perspectives

ORIGINAL ARTICLE OPEN ACCESS

Evaluating Blood–Brain Barrier Permeability, Cytotoxicity, and Activity of Potential Acetylcholinesterase Inhibitors: In Vitro and In Silico Study

L. M. Maboko[1] | A. Theron[2] | J.-L. Panayides[2] | W. Cordier[1] | D. Fisher[3] | V. Steenkamp[1]

[1]Department of Pharmacology, School of Medicine, Faculty of Health Sciences, University of Pretoria, Pretoria, South Africa | [2]Future Production: Chemicals, Council for Scientific and Industrial Research, Pretoria, South Africa | [3]Department of Medical BioSciences, Faculty of Natural Sciences, Neurobiology Research Group, University of Western Cape, Cape Town, South Africa

Correspondence: V. Steenkamp (vanessa.steenkamp@up.ac.za)

Received: 1 July 2024 | **Revised:** 8 November 2024 | **Accepted:** 14 November 2024

Funding: This work was supported by University of Pretoria (608664), Department of Science and Innovation, South Africa, Council for Scientific and Industrial Research, South Africa.

Keywords: acetylcholinesterase inhibition | blood–brain barrier | cytotoxicity | synthetic compounds

ABSTRACT

Acetylcholinesterase inhibitors (AChEIs) remain the first-line treatment for Alzheimer's disease. However, these drugs are largely symptomatic and often associated with adverse effects. This study aimed to evaluate novel pharmacophores for their in vitro AChEI activity, blood–brain barrier (BBB) permeability, and cytotoxic potential, hypothesizing that a combination of AChEIs could enhance symptom management while minimizing toxicity. A library of 1453 synthetic pharmacophores was assessed using in vitro and in silico methods to determine their feasibility as an inhibitor of the AChE enzyme. An in-house miniaturized Ellman's assay determined acellular AChEI activities, while pharmacokinetic properties were evaluated using the SwissADME web tool. The combinational effects of in silico BBB-permeable pharmacophores and donepezil were examined using a checkerboard AChEI assay. Cytotoxicity of active compounds and their synergistic combinations was assessed in SH-SY5Y neuroblastoma and bEnd.5 cells using the sulforhodamine B assay. Cellular AChEI activity of active in silico BBB-permeable predicted compounds was determined using an SH-SY5Y AChE-based assay. An in vitro BBB model was used to assess the effect of compounds on the integrity of the bEnd.5 monolayer. Out of the screened compounds, 12 demonstrated 60% AChEI activity at 5 μM, with compound **A51** showing the lowest IC_{50} (0.20 μM). Five compounds were identified as BBB-permeable, with the donepezil-**C53** combination at ¼IC_{50} exhibiting the strongest synergy (CI = 0.82). Compounds **A136** and **C129**, either alone or with donepezil, showed cytotoxicity. Notably, compound **C53**, both alone and in combination with donepezil, demonstrated high AChEI activity and promising BBB permeability, warranting further investigation.

Abbreviations: %, percentage; °C, degree Celsius; A_b, absorbance of the background; ACh, acetylcholine; AChE, acetylcholinesterase; AChEIs, acetylcholinesterase inhibitors; AD, Alzheimer's disease; A_s, absorbance of the AChE activity signal; ATCC, American Tissue Culture Collection; ATCI, acetylthiocholine iodide; BBB, blood–brain barrier; BOILED-Egg, brain or intestinal estimated permeation; BSA, bovine serum albumin; CI, combination index; CNS, central nervous system; CO_2, carbon dioxide; CSIR, Council for Scientific and Industrial Research; CV, Coefficient of variation; Da, Daltons; DMEM, Dulbecco's modified Eagle medium; DMSO, dimethyl sulfoxide; DTNB, 5,5′-dithiobis(2-nitrobenzoic acid); ECACC, European Collection of Authenticated Cell Cultures; eeAChE, electric eel acetylcholinesterase; ESI, electrospray ionization; *fa*, fraction affected; FCS, fetal calf serum; g, gravitational force; h, hour(s); IC_{50}, half-maximal inhibitory concentration; K_m, substrate concentration; kV, kilovolt; L/h, liter per hour; M, molar; MaxV, maximum velocity; $MaxV_c$, maximum velocity of the negative control; $MaxV_s$, maximum velocity of the sample; mDa, megadalton; $MgCl_2.6H_2O$, magnesium chloride hexahydrate; min, minute(s); mM, millimolar; MS, mass spectrometry; NaCl, sodium chloride; NaOH, sodium hydroxide; nm, nanometers; NMDA, *N*-methyl-D-aspartate; OD, optical density; $OD_{negative}$, optical density of the negative control; OD_{sample}, optical density of the sample; PAS, peripheral anionic site; PBS, phosphate-buffered saline; PC, positive control; Pen-strep, penicillin/streptomycin; pg/mL, picograms per milliliter; P-gp, P-glycoprotein; pH, power of hydrogen; pM, picomolar; RTF, random tree forest; s, second(s); SA, South Africa; SD, standard deviation; SD_b, standard deviation of the background; SD_s, standard deviation of the signal; SEM, standard error of mean; SMILES, simplified molecular input line entry system; SRB, sulforhodamine B; SW, signal window; TCA, trichloroacetic acid; TEER, transendothelial electrical resistance; TNB, 5-thio-2-nitrobenzoate; TPSA, topological polar surface area; Tris–HCl, Tris-hydrochloride; UK, United Kingdom; UPLC, ultra-performance liquid chromatography; USA, United States of America; UV, ultra-violet; V_{max}, maximum velocity; Z′, Z′-factor; μL, microliter; μM, micromolar.

1 | Introduction

Alzheimer's disease (AD) is a progressive neurodegenerative disease affecting the cognitive function of elderly individuals [1]. Since its recognition in 1906, over 55 million people worldwide are estimated to live with AD as of 2023, this number is expected to rise to 152 million by 2050 [2]. The etiology of AD is unclear; however, several theories have been proposed including the amyloid, tangle, cholinergic, and excitotoxicity theories [3]. Of these, the cholinergic theory is the most studied suggesting that acetylcholine (ACh) deficiency caused by cholinergic neuron degeneration and acetylcholinesterase (AChE) activity leads to the cognitive and functional symptoms observed in AD [4].

The AChE enzyme, which breaks down ACh, is the prime pharmacological target for AD. Even though this is well-known, treatment options are limited hence acetylcholinesterase inhibitors (AChEIs) such as donepezil, galantamine, and rivastigmine (Table 1) remain as first-line therapy [5]. However, these drugs only offer symptomatic relief and are used in mild to moderate stages of AD [6]. In addition, AChEIs have side effects, especially during initiation or dose escalation of treatment (Table 1) [7].

Even with known side effects, AChEIs with heterocyclic scaffolds continue to be investigated for AD treatment and this is because dose adjustments may mitigate risks, and the potential benefits could outweigh the risks [16,17]. Heterocyclic compounds, such as *N*-based heterocycles and dimeric tacrine-based inhibitors, have proven to significantly enhance binding affinity and selectivity towards AChE's peripheral anionic site (PAS), improving inhibitory potency [18,19]. Additionally, investigating AChEIs may lead to improved dual-action therapies that maximize benefits while minimizing adverse effects [20].

The combination of AChE-inhibiting heterocyclic compounds with allosteric modulation properties produces a synergistic effect that enhances AChE inhibition [21]. This dual-action therapy could provide both symptomatic and disease-modifying benefits, such as enhancing cholinergic signaling and reducing amyloid plaque formation [22,23]. Furthermore, allosteric modulation of AChE may target multiple neurodegenerative pathways, such as reducing inflammation or preventing excitotoxicity, potentially offering a more comprehensive treatment approach for AD [23].

As AD progresses, AChEIs become less effective and the non-competitive NMDA receptor antagonist memantine becomes the second-line treatment (Table 1) [12]. Memantine is often used in combination with AChEIs (donepezil or rivastigmine), and this combination therapy is more tolerable than monotherapy [24]. Moreover, combination therapy has been shown to delay AD progression by prolonging symptomatic benefits and preserving cognitive function, and it is currently the gold standard for treating moderate to severe AD [25].

Despite the availability of these drugs, treatment for AD with increasing prevalence is still unmet [14]. This leads to the necessity for an ongoing identification of novel effective drugs possessing fewer side effects and better pharmacokinetic properties [14].

TABLE 1 | Current FDA-approved drugs for the treatment of Alzheimer's disease.

Drug name	Chemical structure	Mechanism of action	Clinical effectiveness	Side effects
Donepezil	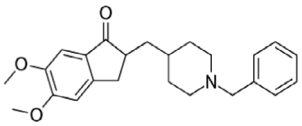	AChEI	Improves memory and attention [8]	Gastrointestinal disorders, nausea, and headache [7]
Rivastigmine	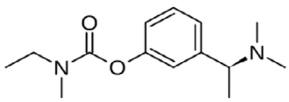	AChEI	Alleviates agitation and mood disturbances [9]	Loss of appetite, vomiting, and dizziness [5]
Galantamine	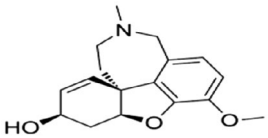	AChEI	Enhances language and communication [10]	Fatigue, weight loss, and heartburn [7]
Memantine	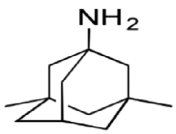	NMDA receptor antagonist	Improve learning and daily functioning [11]	Headache, confusion, and constipation [12]
Aducanumab	$C_{6472}H_{10028}N_{1740}O_{2014}S_{46}$	Anti-Aβ monoclonal antibody	Alleviates memory impairment [13]	Confusion, fever, and delirium [14]
Lecanemab	$C_{6544}H_{10088}N_{1744}O_{2032}S_{46}$	Anti-Aβ monoclonal antibody	Mitigates vascular dysfunction [15]	Disorientation, blurred vision, and back pains [14]

Abbreviations: Aβ, amyloid beta; AChEI, acetylcholinesterase inhibitor; NMDA, *N*-methyl-D-aspartate.

Sadly, drug discovery and development of drugs targeting the central nervous system (CNS) have an overall attrition rate of more than 95% [26]. The high rate of failure is the result of the multifactorial nature of the disease, inefficacy, cytotoxicity, and blood–brain barrier (BBB)-impermeability [27].

Assay development and miniaturization for screening and determining the efficacy of drugs as potential treatments for neurodegenerative diseases has received attention over the course of the last decade. Well-established enzyme based-assays are commonly used to determine activity against targets like cholinesterase, Aβ aggregation, and tau-related protein kinases [28,29]. For AD, the modified Ellman's colorimetric assay is mostly used to assess AChE inhibitory efficacy, and this is due to its cost- and time-effectiveness, reproducibility, and simplicity [30].

Cytotoxicity is a significant hurdle, as nearly a quarter of drug candidates are eliminated from further studies due to toxicity [27]. Common assays that are affordable, rapid, and give an indication of possible toxicity such as the MTT conversion and sulforhodamine B staining are used to assess drug-induced cytotoxicity in cell culture [31]. Additionally, BBB permeability is another challenge in the development of pharmaceuticals designed to treat AD [32]. Due to the ethical aversion to in vivo models and costs, in vitro models such as the bicameral transwell system are used to measure drug penetration [33]. These models, combined with in silico methods, are important for assessing potential drug candidates.

When drugs are found to be inactive, cytotoxic, or BBB-impermeable at early preclinical experimentation, expeditious termination of investigation can occur leading to minimized costs, resources, and time spent on fruitless research [34]. Therefore, assessing a broad spectrum of pharmacophores and their effects in the preclinical stage is of critical importance. The aim of the study was to identify novel synthetic pharmacophores that contain AChEI potential, are non-cytotoxic, and are BBB-permeable. Furthermore, the compound/s adhering to these factors would provide better management of AD symptoms if the combination with an approved AChEI, donepezil, indicated similar or increased activity associated with a decrease in toxicity.

2 | Methods

The experimental design illustrating the methodologies used in this study is provided in Figure 1.

2.1 | Materials

Acetylthiocholine iodide (ATCI), eeAChE from *Electrophorus electricus* (electric eel) type VI-S, acetic acid, acetonitrile, bovine serum albumin (BSA), dimethyl sulfoxide (DMSO), 5,5′-dithiobis(2-nitrobenzoic acid) (DTNB), donepezil, formic acid, galantamine, saponin, SRB stain, trichloroacetic acid (TCA), tris-hydrochloride (HCl), sodium chloride (NaCl), magnesium chloride hexahydrate ($MgCl_2.6H_2O$), and trypan blue were purchased from Sigma-Aldrich (United States of America (USA)). Dulbecco's modified Eagle medium: Ham's F-12 medium (DMEM-Ham's F-12), penicillin/streptomycin (Pen-strep), and fetal calf serum (FCS) were procured from Whitehead Scientific (Pty) Ltd. (South Africa (SA)). Non-essential amino acids, phosphate-buffered saline (PBS), sodium pyruvate, and TrypLE Express Enzyme were purchased from BioWhitakker/Lonza (Thermo-Fischer, USA), BD Bioscience (USA), and GibcoI (Invitrogen, USA), respectively. The human SH-SY5Y neuroblastoma cell line was originally purchased from the American Tissue Culture Collection (ATCC, USA) (ATCC, CRL-2266, RRID:CVCL_0019) by the Department of Pharmacology at the North-West University and was gifted to the Department of Pharmacology at the University of Pretoria, whereas the immortalized mouse brain endothelial (bEnd.5) cell line was purchased from the European Collection of Authenticated Cell Cultures (ECACC, United Kingdom (UK)) (ECACC, Cat no.

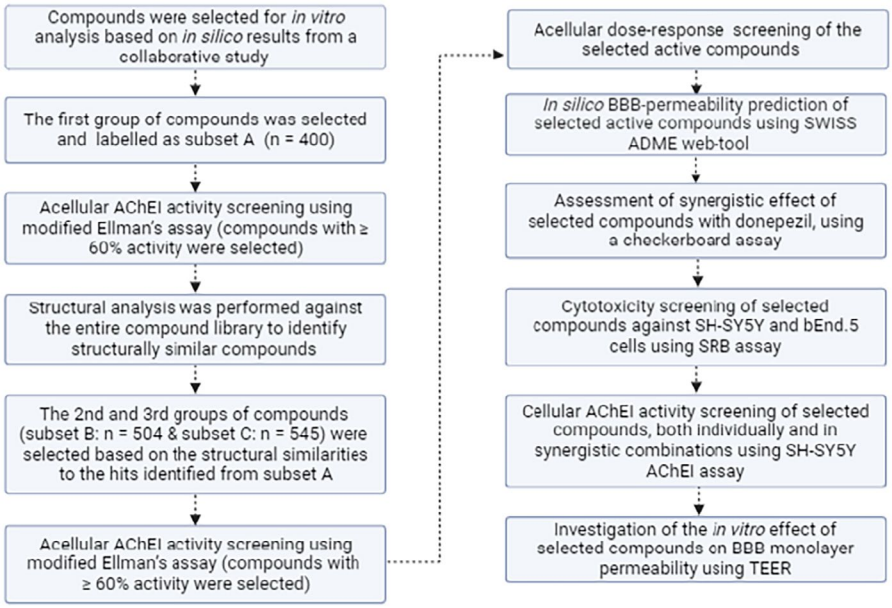

FIGURE 1 | Experimental design illustrating methodologies followed and used in this study.

96091930, RRID:CVCL_2252) by the Department of Medical Biosciences at the University of the Western Cape.

2.2 | Compound Selection and Collection

This study assessed an existing commercial 20000 compound library (Charles River Laboratories/BioFocus, UK) housed at the Council for Scientific and Industrial Research (CSIR) on behalf of the Department of Science and Innovation and the Technology Innovation Agency. The library is stored at −20°C in 96-well plates containing 80 compounds per plate as 10 mM aliquots in DMSO. Three subsets of compounds were selected based on previous work within our collaborative group using computer-aided drug discovery of novel AChEIs [35]. High-throughput virtual screening of the library was employed to predict compounds that are potential AChEIs. Further development of the docking protocol was performed with the use of the Random Tree Forest (RTF) of the SIEVE-Score, which takes into consideration the interaction energies between the ligand and residues in the active pocket. Using this approach, the top 400 compounds were identified using the Schrödinger RTF ($n = 200$) and Qvina RTF ($n = 200$) models, respectively, to form the primary library screen.

Once the hits were identified from the primary screen, structural analysis was performed on the entire library to identify structurally similar compounds that could be subjected to secondary "structure–activity relationship"-like screening. Thus, the second and third subsets (508 and 545 compounds, respectively) were selected based on the structural similarities to the "hits" identified from the first subset. In total, 1453 compounds containing heterocyclic scaffolds albeit with different atom substituents were selected and assayed as three subsets (**A**, **B**, and **C**). Compounds for each subset were numbered with the subset letter as the prefix, followed by the compound number in the subset (e.g., **A1** for compound 1 in subset **A**).

2.3 | Acetylcholinesterase Inhibitory Activity

2.3.1 | Microplate Assay Miniaturization and Optimization

Acetylcholinesterase inhibitory activity was determined using Ellman's method [36], with modifications [37] to the volumes used to accommodate the limited library stock volume. The assay entails the hydrolysis of ATCI by AChE to produce thiocholine, which reacts with DTNB to create the yellow 5-thio-2-nitrobenzoate anion [37].

Apart from the reduced assay volume, the number of buffers was decreased, and a pre- and post-incubation step was included. The ratio and in-reaction concentrations of all constituents were kept as per the original protocol. The three assay buffers were combined into a single mix-buffer (0.045 M Tris–HCl, 0.071 M NaCl, and 0.014 M $MgCl_2.6H_2O$ supplemented with 0.07% BSA, 2.14 mM ATCI, and 2.14 mM DTNB). Degradable reagents (BSA, ATCI, and DTNB) were added on the same day of the assay to avoid the risk of contamination or spontaneous conversion. To allow the reaction to take place, 5 min pre-enzyme and 5 min post-enzyme incubations at room temperature were introduced.

The following was added to a 96-well plate: 10 μL of mix-buffer (blank and negative control), 0.1% DMSO (vehicle control for positive controls), galantamine or donepezil (1 pM to 10 μM; positive controls), or DMSO (0.0001% to 0.5% given its potential enzyme inhibitory potential), as well as 70 μL of mix-buffer. Blank control wells received 70 μL of buffer without DTNB. Plates were incubated for 5 min at room temperature and absorbance was measured spectrophotometrically (ELx800 UV plate reader, BioTek, USA) at 405 nm three times consecutively every 45 s (read-out 1). Thereafter, 20 μL of eeAChE (0.1 U/mL) was added to each well and incubated for 5 min. After the post-enzyme incubation period, absorbance was measured five times consecutively every 45 s (read-out 2). This initial rate kinetic run provided the maximum velocity (MaxV) values for both measurements, from which AChE activity was inferred. Background activity was corrected for by subtracting MaxV values for read-out 1 from read-out 2, after which AChE activity was determined relative to the negative control:

$$\text{AChE activity}\,(\%) = \left(\text{MaxV}_s \,/\, \text{Average MaxV}_c\right) \times 100$$

where MaxV_s is the background-adjusted MaxV of the sample, and Average MaxV_c is the background-adjusted average of the MaxV of the negative control. The concentration providing 50% inhibition (IC_{50}) was obtained from the dose–response curve generated with the use of a log(inhibitor) vs. response function using GraphPad Prism 6 (GraphPad Software, USA).

2.3.2 | Assay Validation

Assay variability, quality, and signal differences were assessed by determining the coefficient of variation (CV), Z'-factor (Z'), and signal window (SW), respectively [38] using the following equations:

$$\text{CV}\,(\%) = \text{SD} \,/\, \text{A} \times 100$$

$$Z' = 1 - \left(3\left[\text{SD}_s + \text{SD}_b\right] / \left[\text{A}_s - \text{A}_b\right]\right)$$

$$\text{SW} = \text{A}_s - \text{A}_b - \left(3\left[\text{SD}_s + \text{SD}_b\right] / \text{SD}_s\right.$$

where A_s and SD_s represent the absorbance and standard deviation of the AChE activity signal, respectively; A_b and SD_b represent the absorbance and standard deviation of the background signal, respectively. Acceptance limits for these parameters were defined as CV ≤ 20%, 0.4 ≤ Z' ≤ 1, and SW ≥ 2. These statistical parameters were used to monitor changes in assay performance during assay miniaturization, optimization, and validation.

2.3.3 | Single-Point and Dose–Response Screening of Compounds

Acetylcholinesterase inhibitory activity of the compounds was determined using the optimized microplate assay protocol as described in Section 2.3.1. A total of 1453 compounds were screened at 5 μM, with a ≥ 60% inhibitory cutoff used to define biologically

active candidates. Blank, negative (mix-buffer), vehicle (0.05% DMSO), and positive controls (5 μM donepezil) were included. Any compounds that were defined as biologically active were further screened between 3200 pM to 32 μM to determine their IC_{50} values.

2.4 | Pharmacokinetic Prediction

Blood-brain barrier permeability of the active compounds was predicted and assessed using the Swiss Institute for Bioinformatics pharmacokinetic prediction tool, SwissADME. Simplified molecular input line entry systems (SMILES) of the compounds were collected from the compound library database. A list of SMILES was then captured using the online SwissADME web tool (http://www.swissadme.ch) [39]. These predictions were done using the brain or intestinal estimated permeation (BOILED)-Egg method, which corresponds to a descriptive graphical approach that discriminates between BBB-permeable and BBB-non-permeable molecules [40]. A compound is predicted to be BBB-permeable if the topological polar surface area (TPSA) is < 80 Å and the WLogP limit is ~6. The yellow and white regions in the BOILED-Egg plot represent BBB and gastrointestinal-permeable compounds, respectively, and thus overlapping areas are considered permeable for both. Blue and red dots are indicative of compounds that are or are not substrates for the P-glycoprotein (P-gp) transporter, respectively [39].

2.5 | Combinational Inhibitory Effects of Compounds With Donepezil

Although both drugs inhibit AChEI, the rationale for the combination was informed by the potential modulation of the catalytic anionic site via binding to the allosteric PAS [41]. The combinational activity of compounds possessing AChEI and donepezil was assessed using the in-house miniaturized assay as described in Section 2.3.1; however, the sample aliquot consisted of the active compound or donepezil alone or in combination at various ratios of their IC_{50} using a checkerboard layout. Nine different combinations of the ¼IC_{50}, ½IC_{50}, and IC_{50} per compound (as shown in Figure S1) were assessed with 5 μL of active compound and donepezil each. The individual compound or donepezil was assessed with a 5 μL sample and 5 μL buffer. The buffer alone at 10 μL was used for the negative control. The fraction affected (*fa*), which relates to the percentage inhibition of the enzyme, of each combination in relation to their individual compounds was analyzed using CompuSyn (PD Science LLC) [42] to generate combination index (CI) values and isobologram based on the median-effect equation, where a CI < 1 indicates synergism, equal to 1 indicates additive activity, and > 1 indicates antagonism.

2.6 | Cytotoxicity Screening of Biologically Active Compounds

2.6.1 | Cell Culture and Maintenance

Human neuroblastoma (SH-SY5Y) and immortalized mouse brain endothelial (bEnd.5) cell lines were cultured in 75 cm^2 cell culture flasks (Greiner Bio-One, USA) using a 1:1 mixture of DMEM and Ham's F-12 nutrient mixture supplemented with 1% pen-strep and 10% heat-inactivated FCS for SH-SY5Y cells, and further supplemented with 1% nonessential amino acids and 1% sodium pyruvate for bEnd.5 cells. Cells were grown to a confluence of ~70% to 80% at 37°C in a humidified incubator (HF212 UV Heal Force, China) with a 5% CO_2 atmosphere, washed with sterile PBS, and chemically detached using TrypLE Express. Detached cells were transferred to a 15 mL centrifuge tube (Thermo-Fischer, USA) together with a 10% FCS-supplemented growth medium to make up the volume. Cells were centrifuged (Allegra X-22 centrifuge, Beckman Coulter, USA) at 200 *g* (SH-SY5Y) or 700 *g* (bEnd.5) for 5 min. The supernatant was discarded, and the pellet was re-suspended in 1 mL of 10% FCS-supplemented medium. Cells were counted using the trypan blue exclusion assay (0.4% *w/v*) and diluted to 5×10^4 or 400×10^4 cells/mL (SH-SY-5Y; 96-and 24-well plates) and 1.5×10^4 or 50×10^4 cells/mL (bEnd.5; 96-and 24-well plates) in 10% FCS-supplemented growth medium.

2.6.2 | Cell Seeding and Compound Exposure

A volume of 100 μL of cell suspension was seeded into sterile round-bottomed 96-well plates (Sigma-Aldrich, USA) at a seeding density of 5000 and 1500 cells/well for SH-SYSY and bEnd.5 cells, respectively. Seeded plates were incubated overnight at 37°C in an atmosphere of 5% CO_2 to allow for cell attachment. Attached cells were exposed to 100 μL medium (negative control), 1% DMSO (vehicle control), 1% saponin (positive control), donepezil (1000 pM to 100 μM), or the biologically active in silico BBB-permeable compounds (1000 pM to 100 μM) prepared in serum-free medium. Plates were incubated at 37°C in a humidified incubator with 5% CO_2 for 72 h.

2.6.3 | Sulforhodamine B Colorimetric Assay

The cytotoxicity of the compounds was assessed by cell density determination using the SRB staining assay as described by Vichai & Kirtikara [43] with minor changes to volumes used.

After the exposure period, 50 μL of a 50% TCA solution was added to each well and the plates were incubated at 4°C for 24 h. After fixation, plates were washed three times with slow-running tap water and dried in an oven (EcoTherm, Labotec, South Africa) at 40°C–45°C. A volume of 100 μL of 0.057% SRB solution was added to each well and the plates were incubated at room temperature for 30 min in the dark. After 30 min, the unbound dye was removed by washing the plates three times with 150 μL of 1% acetic acid and dried in the oven.

The bound dye was extracted from fixed cells by adding 200 μL of 10 mM Tris-base solution (pH 10.5) to each well. Plates were shaken on a gyratory shaker (VRN-200, Gemmy Industrial Corporation, Taiwan) for 1 h to solubilize the protein-bound dye. After the dye had been solubilized, the optical density (OD) was measured at 540 nm (reference: 630 nm) using an ELX800 microplate reader (BioTek Instruments Inc., Highland Park, USA). All values were blank-subtracted, and the cell density (%) was calculated using the formula below:

$$\text{Cell density (\% relative to negative control)} = OD_{sample} / \text{Average } OD_{negative} \times 100$$

Where "OD_{sample}" refers to the corrected optical density of the sample and "$OD_{negative}$" is the corrected optical density of the negative control.

2.7 | Michaelis–Menten Kinetics Assay

The Michaelis–Menten kinetics of the non-cytotoxic, AChEI active, in silico BBB-permeable compounds were determined as per Section 2.3.1; however, compounds were tested at the IC_{50} against a substrate concentration range (ATCI; 0 to 2.14 mM). The negative control consisted of a mix buffer to determine the upper plateau of enzyme saturation. Two additional controls were included to monitor inter-reagent interactions: DTNB without ATCI, and ATCI without DTNB. The substrate concentration at half the maximum reaction rate (K_m) versus the reaction rate (measured maximum velocity of reaction at each concentration being equivalent to initial velocity, where acceleration/gradient is steepest, to obtain the maximum velocity [V_{max}] at the concentration with the highest initial velocity) was plotted using GraphPad Prism 6 (GraphPad Software, USA). Results were further processed as Lineweaver–Burk plots and enzyme inhibition mechanisms can be classified as either competitive, non-competitive, or mixed (as shown in Figure S2).

2.8 | Chemical Stability Analysis

The non-cytotoxic, AChEI active, in silico BBB-permeable compounds were subjected to quality control analysis using ultra-performance liquid chromatography (UPLC) coupled to exact mass spectrometry (MS), to ensure chemical integrity. Quality control analysis was conducted at the CSIR. A Waters UPLC coupled in series to a Waters SYNAPT G1 HDMS mass spectrometer was used to generate accurate mass data. Optimization of the chromatographic separation was done using a Waters HSS T3 C18 column (150 × 2.1 mm, 1.8 μm) and the column temperature was controlled at 60°C. A binary solvent mixture consisting of water (eluent A) containing 10 mM formic acid (natural pH of 2.4) and acetonitrile (eluent B) containing 10 mM formic acid was employed. The initial conditions were 95% A at a flow rate of 0.4 mL/min which was maintained for 30 s, followed by a linear gradient to 5% A at 6 min. The conditions were kept constant for 1 min and then reverted to the initial conditions. The runtime was 10 min, and the injection volume was 1 μL. Samples were kept at 6°C in the Waters Sample Manager during the analysis.

The SYNAPT G1 mass spectrometer was used in V-optics and electrospray mode to enable the detection of all electrospray ionization (ESI)-compatible compounds. Leucine enkephalin (50 pg/mL) was used as a reference calibrant (Lock Mass) to obtain typical mass accuracies between 1 and 5 mDa. The mass spectrometer was operated in both ESI-positive and -negative modes with a capillary voltage of 2.0 kV, the sampling cone was set at 30 V and the extraction cone at 4.0 V. The scan time was 0.1 s covering the 50–1000 Da mass range, with an interscan time of 0.02 s. The source temperature was 120°C and the desolvation temperature was set at 450°C. Nitrogen gas was used as the nebulization gas at a flow rate of 550 L/h and cone gas was added at 50 L/h. The software used to control the hyphenated system and to do all data manipulation was MassLynx 4.1 (SCN 872).

A Waters UPLC photodiode array detector was operated in front of the mass spectrometer without any splitting of the column eluent. The detector was operated in full scan mode covering the 200–500 nm wavelength range with a wavelength accuracy of 1.2 nm.

Each compound was analyzed in both positive and negative ionization modes and full-scan ultraviolet (UV) data were collected simultaneously. The data were first evaluated to determine whether the compound is preferably ionized in ESI-positive or ESI-negative mode. The best ionization mode was selected, and the presence of the target compound was confirmed. Thereafter the UV data was evaluated to determine whether the compound contained chromophores and displayed a usable UV spectrum. For compounds that were UV-active, a MaxPlot chromatogram was evaluated, and all relevant compounds were integrated to determine the purity of the target compound.

2.9 | In Situ Acetylcholinesterase Inhibitory Activity of Compounds

The assay was carried out according to the method of Ellman et al. [36] and Eldeen et al. [37] as described in Section 2.3.1 with minor modifications. SH-SY5Y cells were cultured and seeded as described in Section 2.6.1; however, cells were seeded at 400000 cells/well in a 24-well plate. After the cells had attached, the culture medium was aspirated and replenished with 300 μL of the specific compound in buffer at 1.5/IC_{50}, IC_{50}, and 1.5 × IC_{50} and incubated for 5 min at room temperature. Post-exposure, 100 μL mix-buffer (pH 8) containing aqueous 0.045 M Tris–HCl, 0.050 M NaCl, and 0.010 M $MgCl_2.6H_2O$ supplemented with 0.05% BSA, 1.5 mM ATCI and 3 mM DTNB was added. Plates were incubated for 5 min and read spectrophotometrically at 405 nm over a 1 h period at 3 min intervals. The AChE activity was determined relative to the negative control (as per Section 2.3.1).

2.10 | In Vitro Effect on Blood–Brain Barrier Permeability

2.10.1 | The In Vitro Bicameral System

The bicameral chamber system was used for the in vitro model of BBB permeability, where the basolateral side of the well assumes the abluminal side of the capillary endothelium, while the apical chamber (i.e., the insert) assumes the luminal side of the capillary. The measurement was performed as described by Srinivasan et al. [44]. The in vitro BBB model was used to determine bEnd.5 peak values and the effect of three biologically active in silico BBB-permeable, non-cytotoxic compounds on bEnd.5 monolayer transendothelial electrical resistance (TEER).

The bEnd.5 cells were cultured and maintained as described in Section 2.6.1. A volume of 300 μL bEnd.5 cell suspension was seeded at a density of 50000 cells into the apical chamber

of a Transwell insert (pore size of 0.45 μm, filtration diameter of 12 mm, and an effective surface area of 0.6 cm^2) (Merck-Millipore, UK) placed in sterile 24-well plates (Bio-Smart Scientific, SA). An aliquot of 500 μL growth medium was pipetted in the basolateral well. Plates were incubated at 37°C and 5% CO_2 for 24 h to attain cell confluence.

The TEER peak values after 24 h seeding incubation were measured using the EVOM TEER measurement system (Millipore, Germany) daily for 6 days, with the medium changed daily after measurement. The measurement was performed by connecting the electrodes to either side of the cell monolayer and measuring the resistance. The resistance of the blank (inserts without cells) was subtracted from the resistance value of the cell monolayer (inserts with cells), and the resultant value was multiplied by the surface area of the inserts to standardize the TEER value. The effect of the compounds on monolayers of bEnd.5 endothelial monolayer permeability was assessed by determining the TEER. Plates were incubated at 37°C, and 5% CO_2 while TEER was carried out and monitored for 12, 24, and 48 h periods.

2.11 | Statistical Analysis

Experiments were conducted with technical and biological triplicates to obtain nine data points per test. All data processing was conducted using Microsoft Office Excel 2019 (Microsoft, USA) and GraphPad Prism 6 (GraphPad, Software, USA). Data points estimated to be outliers were excluded using Grubb's testing. The IC_{50} was calculated by nonlinear regression analysis of the response-concentration (log) curve. Results were reported as mean ± standard error of the mean (SEM). The student's *t*-test was used to determine significance ($p < 0.05$) relative to the comparator.

3 | Results

3.1 | Acetylcholinesterase Inhibitory Activity

3.1.1 | Assay Miniaturization and Optimization

Donepezil and galantamine, known AChE inhibitors, were used in the development, optimization, and validation of the miniaturized AChE assay as positive controls. Both compounds inhibited AChE dose-dependently, with donepezil displaying greater potency (IC_{50} of 0.06 ± 0.07 μM) compared to galantamine (IC_{50} of 1.99 ± 0.10 μM). The potential inhibitory activity of DMSO was assessed to account for potential confoundment. Concentrations ≥ 0.1% DMSO significantly ($p < 0.05$) inhibited AChE by ≥ 21%, thus limiting the testing concentration to 5 μM. Validation parameters were within acceptable ranges: CV ≤ 20%, Z′ ≥ 0.5 but < 1 and SW ≥ 2.

3.1.2 | Acetylcholinesterase Inhibitory Activity Screening of the Compounds

Compounds with ≥ 60% AChEI activity were considered biologically active. Such compounds were only present in subsets **A** and **C** (Figure 2A,B). Of the 400 compounds from subset **A**, only six compounds (**A8**, **A51**, **A73**, **A136**, **A175**, and **A176**) were considered biologically active (Figure 2A). All active compounds, apart from compound **A8**, contained a donepezil-like scaffold, benzo-fused heterocycle, albeit with different atom substituents within itself (Table 2).

Structural analysis was performed on the entire compound library to identify compounds that were structurally similar to actives of subset **A**. Additionally, in silico BBB permeability predictions were performed to refine the selection of these subsets. Subsets **B** and **C** were selected based on their structural similarities and BBB-permeability predictions to actives **A8** and **A73**, respectively. Subset **B** ($n = 508$) was excluded due to inactivity. Six compounds (**C33**, **C43**, **C53**, **C82**, **C129**, and **C189**) from subset **C** ($n = 545$) were determined to be active (Figure 1B). Active compounds identified from subset **C** possessed the imidazo[1,2-*a*]pyridine scaffold similar to the parent compound **A73** (Table 3), which is a subset of the aforementioned benzo-fused heterocycles.

The 12 active compounds were further analyzed to determine their AChEI IC_{50} values. Of the six active compounds in subset **A**, **A51** was the most promising compound as it had an IC_{50} value of 0.20 μM (Table 4). For subset **C**, **C129** was found to be the least active ($IC_{50} = 12.52$ μM). None of the compounds achieved an AChEI potency comparable to that of donepezil, with IC_{50} inhibitory activities being 6.7- to 556.0-fold lower than any of the actives.

3.2 | Pharmacokinetics Prediction

Based on the BOILED-Egg results of the 12 compounds with AChEI activity ≥ 60% (Figure 3), five compounds (**A8**, **A73**, **A136**, **C53**, and **C129**) were predicted to be BBB-permeable, whereas, seven compounds (including **A51**), were predicted as BBB-impermeable. Of the five compounds predicted to be BBB-permeable, only two, **A8** and **A136**, were found to be P-gp substrates.

3.3 | Combinational Treatment Effects

The five compounds with AChEI activity and predicted BBB permeability (**A8**, **A73**, **A136**, **C53**, and **C129**) were combined with donepezil at their ¼IC_{50}s, ½IC_{50}s, and IC_{50}s. A total of 45 combinations were assessed with five combinations displaying synergistic activity, 15 combinations antagonistic activity, and 25 combinations additive activity as shown in Table S1 and isobologram (Figures S3–S7). In this study, the focus was on the combinations with synergistic activity (CI < 1), which was observed between: ¼IC_{50} donepezil and ½IC_{50} **A136** (CI = 0.61); ¼IC_{50} donepezil and IC_{50} **A136** (CI = 0.81); ½IC_{50} donepezil and ½IC_{50} **A136** (CI = 0.81); ½IC_{50} donepezil and IC_{50} **A136** (CI = 0.69); ¼IC_{50} donepezil and ¼IC_{50} **C53** (CI = 0.82).

3.4 | Cytotoxicity Screening

Most of the compounds with AChEI activity which indicated BBB permeability, except for **A136** and **C129**, presented with a cell density > 100% over a concentration range of 0.001 and 10 μM after the 72 h incubation period (Figure 4). At a concentration of

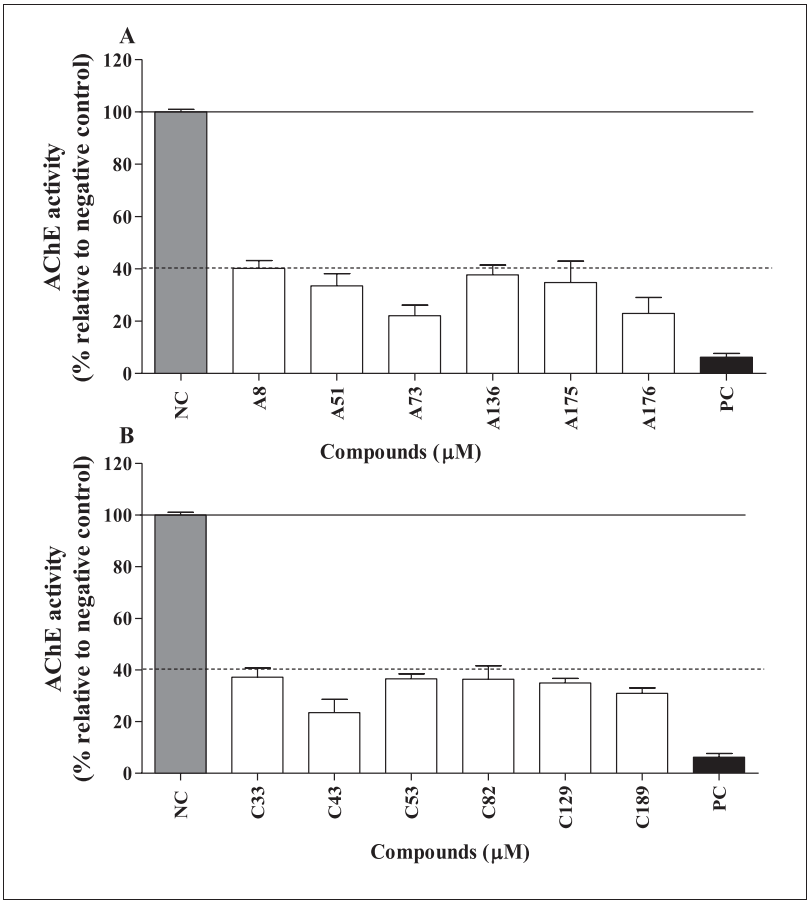

FIGURE 2 | The acetylcholinesterase inhibitory activity of compounds from subsets **A** and **C** indicating activity ≥ 60%. The solid line indicates 100% acetylcholinesterase activity, whereas the dotted line indicates 40% acetylcholinesterase activity (selected bioactive threshold). NC, Negative control; PC, Positive control (donepezil, 5 μM).

100 μM, **A8**'s effect on cell density was comparable to the negative control (> 100%), while **A73** and **C53** displayed low cytotoxicity at 100 μM, with a cell density reduction of 27% and 49%, respectively. Donepezil and **C129** were found to be cytotoxic, with IC_{50} values of 43.00 and 13.64 μM, respectively, resulting in cell reduction of 90.76 and 65.86%, respectively, at 100 μM. Although **A136** increased cell density (> 100%) between 1 and 3.2 μM, it obliterated the cells at concentrations ≥ 10 μM. **A136** was considered the most cytotoxic with an IC_{50} of 4.99 μM.

Of the five synergistic combinations, the combination of **C53** (¼IC_{50}) and donepezil (¼IC_{50}) was the least cytotoxic with a cell density reduction of 23% (Figure 5). However, it should be noted that the cytotoxicity of the combination (compound plus donepezil) was higher than that of the individual compounds. As the combinations of **A136** and donepezil indicated cytotoxicity, these were not investigated further, irrespective of their strong synergistic effect.

Compounds **A8**, **A73**, and **C53**, did not affect cell density at the concentrations tested and were further assessed for their purity and stability using UPLC-MS to identify if any decomposition of the compounds had occurred since the library was purchased. No degradation or decomposition was noted for the three compounds (stored at −20°C) over time.

Prior to assessing the effect of the compounds which were found to be non-cytotoxic against SH-SY5Y cells on the integrity of endothelial monolayers, the cytotoxicity of these compounds in bEnd.5 cells was investigated. All compounds including the synergistic combinations resulted in a cell density > 100% at concentrations of 0.001 to 10 μM (Figure S8). At concentrations ≥ 10 μM, the effect of compounds **A8** and **A73** on bEnd.5 cell density was comparable to the negative control (> 100%), while donepezil and **C53** displayed negligible cytotoxicity at 100 μM (36% and 10%, respectively).

The synergistic combination of **C53** [¼IC_{50}] and donepezil [¼IC_{50}] resulted in bEnd.5 cell density (> 100%) comparable to the negative control (Figure S9). The low cytotoxicity observed in both cell lines, along with the BBB permeability and AChEI activity of A8, A73, and C53, as well as the synergistic combination of C53 (¼IC50) and donepezil (¼IC50), make these compounds ideal candidates for further drug development investigations.

3.5 | Inhibition Kinetics of Acetylcholinesterase Enzyme

Michaelis–Menten kinetics was used to determine the mode of AChEI inhibition, which was confirmed by the Lineweaver–Burk

TABLE 2 | Compounds in subset A that inhibited acetylcholinesterase activity by ≥ 60%.

Main scaffold: benzo-fused heterocycle core		
	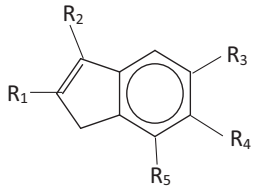	
Compound	**Chemical structure and formula**	**AChE inhibition (%) ± SEM**
A8	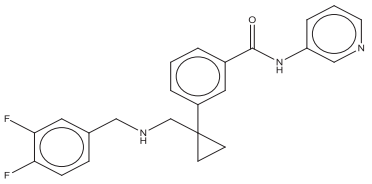 C23H21F2N3O	59.87 ± 3.04
A51	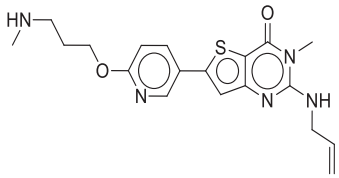 C20H25N5O2S	66.53 ± 4.67
A73	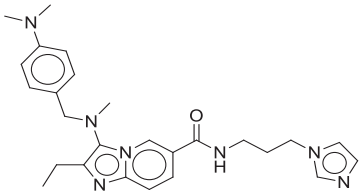 C26H33N7O	77.98 ± 4.13
A136	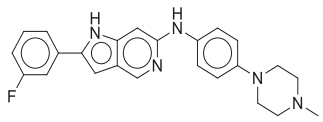 C24H24FN5	62.33 ± 3.75
A175	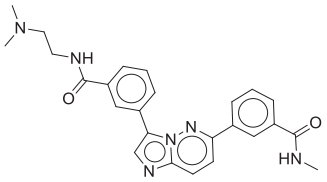 C25H26N6O2	65.28 ± 8.20
A176	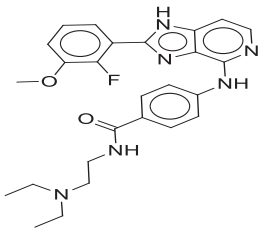 C26H29FN6O2	77.08 ± 6.09

TABLE 3 | Compounds in subset C that inhibited acetylcholinesterase activity by ≥60%.

Scaffold: imidazo[1,2-*a*]pyridine

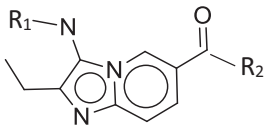

Compound	Chemical structure and formula	AChE inhibition (%) ± SEM
C33	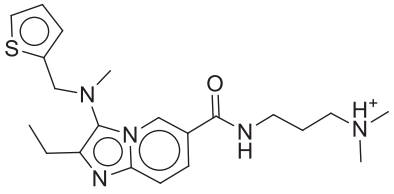 C21H30N5OS+	62.77 ± 3.50
C43	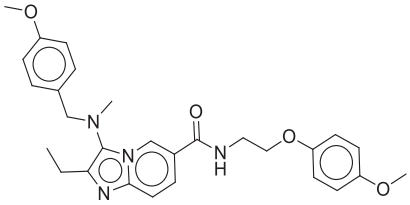 C28H32N4O4	72.16 ± 3.14
C53	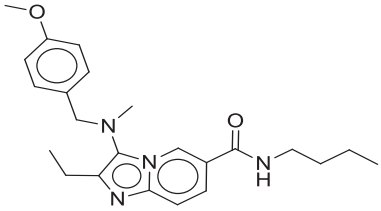 C23H30N4O2	63.41 ± 1.89
C82	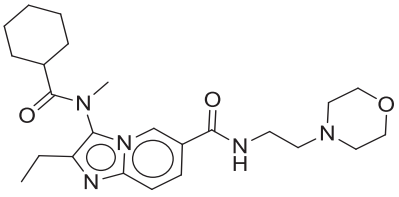 C24H35N5O3	68.66 ± 1.87
C129	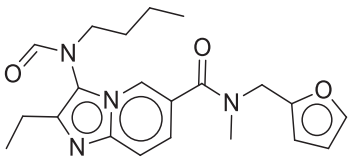 C21H26N4O3	65.03 ± 1.75
C189	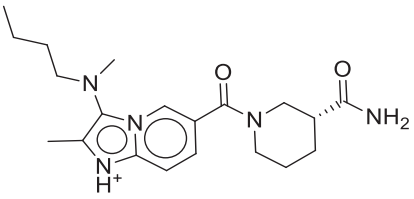 C20H30N5O2+	69.00 ± 2.04

plots. The known AChEI, donepezil, displayed mixed competitive and non-competitive inhibition (Figure S10A). Compound **A8** was an uncompetitive inhibitor (Figure S10B), whereas **A73** and **C53** displayed mixed inhibition (Figures S10C,D).

TABLE 4 | Acetylcholinesterase half maximal inhibitory concentration values and coefficient correlation of active compounds.

Compounds	AChE IC_{50} values ± SEM (μM)	R^2
A8	5.86 ± 0.01	0.88
A51	0.20 ± 0.06	0.86
A73	3.56 ± 0.09	0.89
A136	16.68 ± 0.04	0.87
A175	15.37 ± 0.23	0.78
A176	2.78 ± 0.08	0.93
C33	3.71 ± 014	0.80
C43	3.37 ± 0.11	0.87
C53	3.36 ± 0.12	0.85
C82	7.34 ± 0.14	0.88
C129	12.52 ± 0.12	0.92
C189	4.49 ± 0.08	0.86
Donepezil	0.03 ± 0.04	0.89

Abbreviations: IC_{50}, concentration resulting in 50% inhibitory effect; R^2, correlation coefficient; SEM, standard error of the mean.

3.6 | In Situ Acetylcholinesterase Inhibitory Activity of Compounds

Donepezil significantly ($p < 0.1$ and $p < 0.001$) inhibited AChE at all concentrations with the IC_{50} and $1.5 \times IC_{50}$ showing comparable inhibition of 68% and 67%, respectively. Compound **A8** at the concentrations of $1.5/IC_{50}$ and IC_{50} had a similar reduction of 20% and 28%, however, the $1.5 \times IC_{50}$ did not display any AChE inhibition (Figure 6). Although **A73** possessed a dose–response inhibitory response, a maximum of 10% reduction at IC_{50} was noted. Similar to donepezil at all concentrations ($1.5/IC_{50}$, IC_{50}, and $1.5 \times IC_{50}$), **C53** significantly ($p < 0.01$, $p < 0.001$, and $p < 0.0001$) inhibited AChE by 40%, 61%, and 60%, respectively (Figure 5), suggesting a plateaued effect at higher concentrations. The combination of **C53** ($¼IC_{50}$) and donepezil ($¼IC_{50}$) inhibited AChE significantly ($p < 0.1$) by 69% compared to the individual compounds (Figure S11). **C53**, both as a single treatment and in combination with donepezil, demonstrates strong potential as an ideal candidate for further drug development investigations.

3.7 | In Vitro Effect on Blood–Brain Barrier Permeability

The effect of the compounds that were AChEI active and non-cytotoxic was assessed using TEER measurement. The TEER measurements across the control monolayers followed a typical profile for bEnd.5 endothelial monolayer with a biphasic response where TEER initially increases to a peak at Day 0–3, plateaus on Day 3–4 and then gradually decreases on Day 5–6 [45]. After 12 h of exposure, neither donepezil, **A8**, **A73**, or the combination of donepezil and **C53** at both concentrations (IC_{50} and

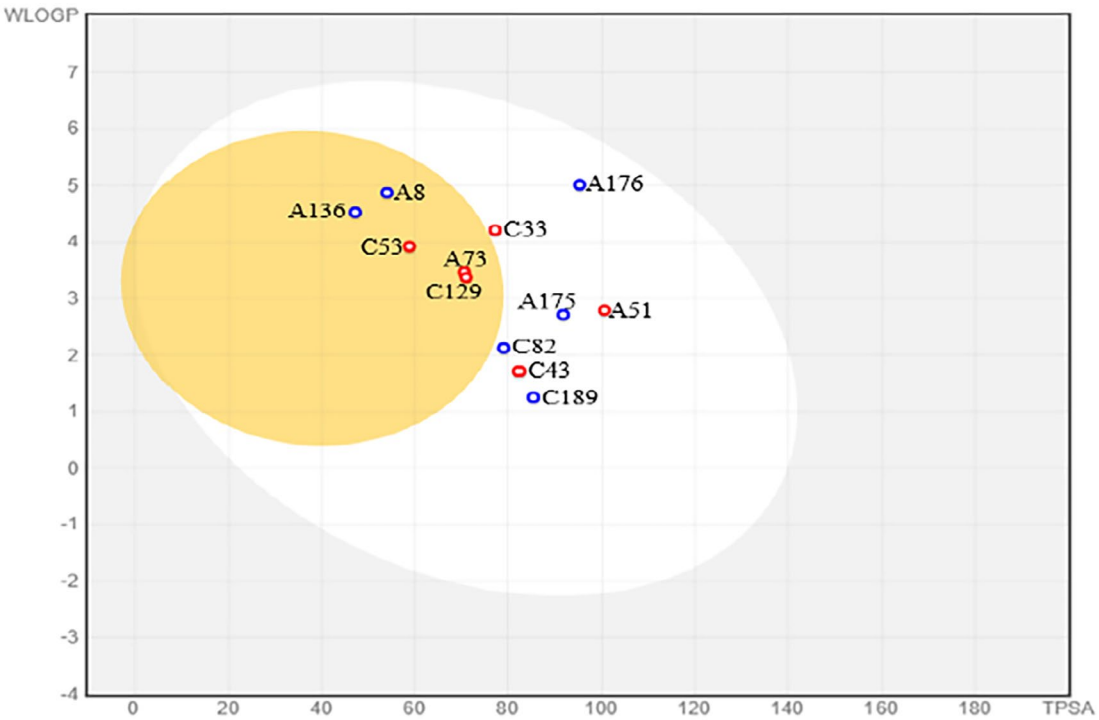

FIGURE 3 | A brain and intestinal predicted permeation plot of the 12 compounds with acetylcholinesterase inhibitory activity. The compounds in the yellow circle are considered blood–brain barrier permeable, and those in the white circle as gastrointestinal-permeable. The compounds with a blue circle are predicted to be P-gp substrates, whereas those with a red circle are not P-gp substrates.

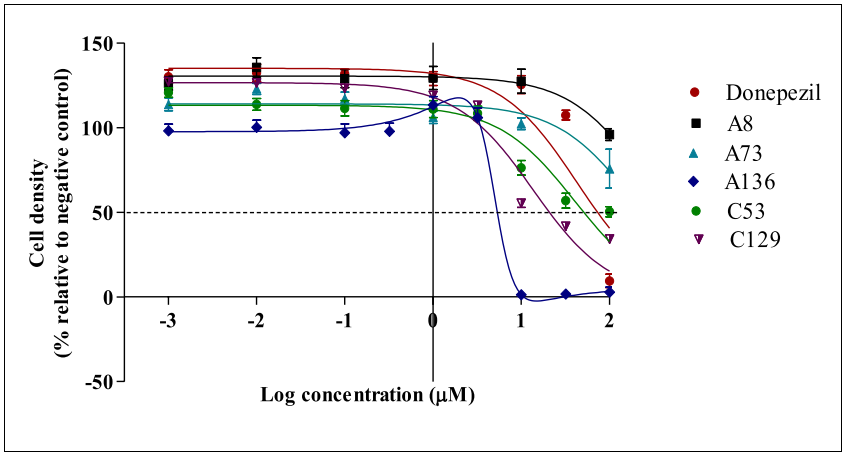

FIGURE 4 | The effect of the compounds with acetylcholinesterase inhibitory activity on SH-SY5Y cell density after 72 h exposure.

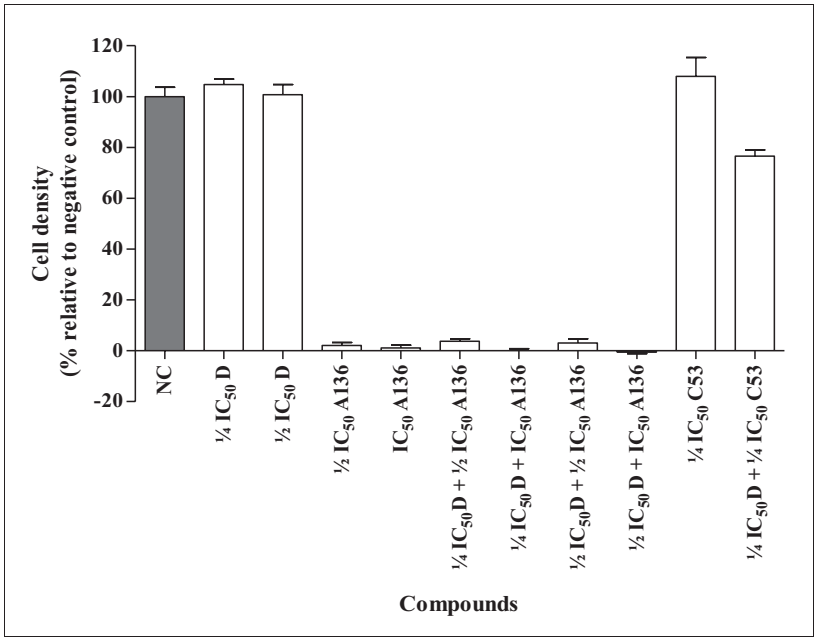

FIGURE 5 | Effect of the compounds which indicated synergistic potential (CI < 1) on SH-SY5Y cell density, when tested alone or in combination. D, Donepezil; IC_{50}, concentration resulting in 50% inhibition; NC, negative control.

$1.5 \times IC_{50}$) displayed any significant difference in TEER values when compared to the negative control, whereas compound **C53** significantly increased ($p < 0.001$) the endothelial resistance at $1.5 \times IC_{50}$ (Figure 7).

A73 (IC_{50} and $1.5 \times IC_{50}$), **C53** (IC_{50} and $1.5 \times IC_{50}$), and the combination of donepezil and **C53** showed TEER comparable to the negative control after 24 h and significantly increased ($p < 0.001$) after 48 h. Donepezil and **A8** at $1.5 \times IC_{50}$ also significantly ($p < 0.01$ and $p < 0.001$, respectively) elevated TEER of bEnd.5 monolayers after 48 h exposure.

4 | Discussion and Conclusions

In this study, the AChE microplate assay was modified, optimized, and validated, preserving the robustness of Ellman's method with Eldeen's modifications, while developing a single assay buffer using a reduced volume. As in this study, single buffers were also utilized by Ingkaninan et al. [46].

The total assay volume was reduced from 250 to 100 μL. Similarly, Ffrench-Constant & Bonning [47] reduced assay volumes to 200 and 55 μL, respectively, while maintaining reproducibility. Despite changes such as using a single buffer instead of three, reducing assay volume, or altering substrate concentrations, the potency of donepezil and galantamine remained consistent with the original method [41]. These results confirmed that the AChE assay was successfully miniaturized and optimized in this study. With all statistical parameters within acceptable ranges, this assay was used to screen a large number of compounds. A final concentration of 0.05% DMSO was determined to be suitable for AChE assays. These findings are consistent with those of Kumar & Darreh-Shori [48] and Novales &

Schwans [49], highlighting the importance of assessing solvent compatibility in in vitro studies [38].

Heterocyclic scaffolds, particularly the benzo-fused heterocycles found in subset **A** compounds, are recognized as essential structural backbones for novel drugs used to treat a range of diseases [50]. Despite their widespread use in treating various conditions, their application in drugs targeting neurodegenerative diseases like AD remains limited, possibly due to unfavorable physicochemical properties [51]. In contrast, the imidazo[1,2-a]pyridine scaffold, present in the active compounds of subset C, is regarded as one of the most potent bicyclic 5–6 heterocyclic rings and is classified as a "drug prejudice" scaffold [52]. This is because it frequently appears in the lead discovery of novel synthetic drugs targeting a variety of mechanisms, including AChE inhibition [53]. Gurjar et al. [54] reported cholinesterase inhibitory activity in designed imidazole derivatives, and while the structures in this study are not identical to those reported, the scaffolds are likely to have contributed to the observed AChEI activity.

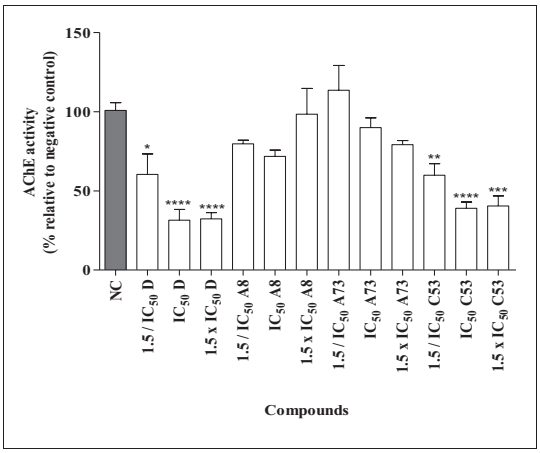

FIGURE 6 | Cellular acetylcholinesterase inhibitory activity of compounds with potential acellular acetylcholinesterase inhibitory activity. Significance of inhibition relative to negative control is indicated as $*p<0.1$, $**p<0.01$, $***p<0.001$, $****p<0.0001$. D, Donepezil; IC_{50}, concentration resulting in 50% inhibition; NC, negative control. The compounds were screened at the concentrations of $1.5/IC_{50}$, IC_{50}, and $1.5\times IC_{50}$.

In addition to efficacy, favorable pharmacokinetic parameters of potential drugs are evaluated early in the drug discovery process [55]. In this study, of the five compounds (**A8**, **A73**, **A136**, **C53**, and **C129**) predicted to be BBB-permeable, **A8** and **C129** emerged as the most promising leads due to their parameters falling squarely within the optimal range for BBB permeability. Among the predicted BBB-permeable compounds, **A8** and **A136** were identified as P-gp substrates. The P-gp transporter can reduce the CNS availability of these compounds by actively transporting lipophilic substances back into the bloodstream, making this an important pharmacokinetic factor to consider during drug development [56].

There is increasing interest in combination therapy at lower dosing regimens, with the primary goal being to achieve a synergistic effect, or a "booster" effect, that enhances drug efficacy [57]. In this study, the greatest synergistic effect (CI = 0.61) was observed when the high AChE inhibitor, donepezil, was combined with a low AChE inhibitory compound (**A136**). This synergy may result from the synthetic pharmacophores binding allosterically to the PAS of AChE [21]. Additionally, it has been noted that synergistic activity is often observed when lower concentrations of each compound are combined [58]. This concept aligns with the synergistic effect

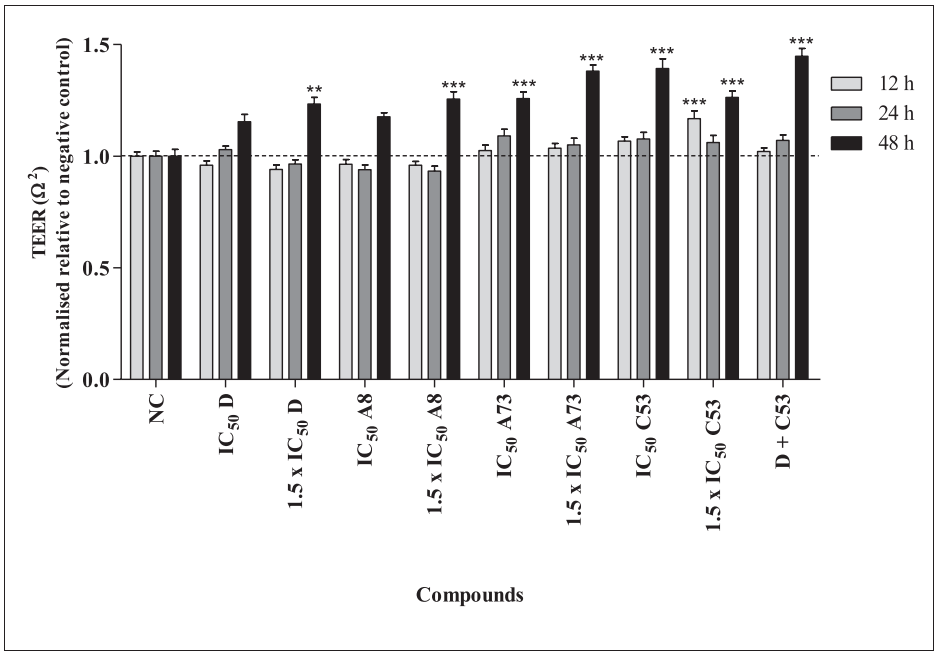

FIGURE 7 | The effect of the compounds that were non-cytotoxic and contained acetylcholinesterase inhibitory activity, on bEnd.5 monolayer permeability (TEER) after 12, 24, and 48 h treatment. The significance of changes relative to the negative control is indicated as $**p<0.01$, $***p<0.001$. IC_{50}, concentration resulting in 50% inhibition; D, Donepezil; NC, negative control.

seen in this study between donepezil and **C53** at their lowest concentrations (¼IC_{50}). For systematic comparison and further support of these findings, isobolographic experiments need to be performed to determine the dose–response relationship of the drugs in combination. Further explanation of the observed effects in relation to the mechanism of inhibition is provided later in the study.

To ensure the viability of neuronal-targeting drugs, toxicity must also be evaluated. Among the active in silico BBB-permeable compounds, **A136** and **C129** were found to be cytotoxic, with **A136** exhibiting a hormetic effect at lower concentrations. Researchers such as Mattson & Cheng [59] and Pallàs et al. [60] suggest that hormesis could result from the activation of cell-survival signaling kinases. Additionally, Demirovic & Rattan [61] reported that the hormetic dose–response may occur through the oxidative stress response pathway and antioxidant response element. These mechanisms may explain the hormetic effect observed with **A136**. Although **A136** and **C129** effectively inhibited AChE activity, these compounds, along with the combination of **A136** and donepezil (despite their strong synergistic effect), were excluded from further investigation due to their cytotoxicity.

All compounds exhibited lower cytotoxicity in bEnd.5 cells compared to SH-SY5Y cells, which is consistent with findings by Zaremba-Czogalla et al. [62] and Michaelis et al. [63]. This difference may be attributed to metabolic alterations in tumor cells and compromised membrane integrity, making them more susceptible to compound toxicity than "normal" cells [64]. In contrast, non-cancerous cells, particularly endothelial cells, possess additional defense mechanisms against prolonged exposure to toxins or stress-inducing agents [63]. These observations highlight the importance of assessing cytotoxicity in at least two cell lines during the early stages of CNS-targeting drug discovery.

Determining a potential candidate's mechanism of action is a crucial step in the drug discovery process [65]. Compound **A8** was identified as an uncompetitive inhibitor, meaning it binds specifically to the enzyme-substrate complex [66]. In contrast, similar to donepezil, **A73** and **C53** exhibited mixed inhibition, indicating that these compounds can bind to both the active site of the free enzyme and the enzyme-substrate complex to achieve the desired effect [67]. The synergistic effect observed with the donepezil-**C53** combination at the lowest concentration may be due to allosteric binding at the PAS. This suggests that lower doses of each compound can produce synergistic combinations, potentially mitigating cytotoxicity and side effects associated with higher doses of single drugs [57].

The AChEI activity observed for the compounds in this study, particularly at IC_{50} and $1.5 \times IC_{50}$, may be attributed to differences between the acellular and cellular environments. Additionally, variations in factors such as binding affinity and steric arrangement within the active site can lead to species-specific differences in inhibitory activity and sensitivity distributions [68]. Based on the results, it appears that compounds **A8** and **A73** may selectively and more effectively inhibit the electric eel form of AChE rather than the human AChE enzyme, suggesting that these compounds may not exhibit significant AChE inhibition in vivo.

Immortalized brain endothelial cells (BECs) are reported to mimic the BBB closely, especially because of their, expression of tight junction (TJ) proteins, and other BBB-specific proteins [69]. This bEnd.5 BECs were cultured to grow monolayers in bicameral chambers, and TEER was measured across the monolayers to evaluate the permeability. In this study, all compounds including the combination, increased the TEER over 48-h exposure, suggesting that they effectively decreased the permeability across the in vitro BBB monolayer [70]. This might be due to the fact that the treatment of bEnd.5 cells with these compounds may have led to endogenous antioxidant production and/or increased TJ protein expression may have been responsible for the decreased permeability across the bEnd.5 cell monolayers [45,71]. Decreased permeability could be interpreted as indicative of a tighter more impermeable brain capillary endothelium, which is counter neurodegenerative pathology. Consequently, ion transportation across the BBB may be improved as leak currents across paracellular pathways, driven by passive ionic fluxes could be substantially arrested. This novel effect on the brain capillary endothelium must be seen as an additional positive characteristic of these selected pharmaceuticals.

Additionally, the in vitro permeation of the compounds through the BBB monolayer was assessed as a preliminary investigation using UPLC-MS. Preliminary results indicated that compounds **A8**, **A73**, **C53**, and the donepezil-**C53** combination (Figures S12–S17) were detected in both the apical and basolateral chambers of the in vitro BBB monolayer model, suggesting that they successfully permeated the barrier. These results suggested that permeation of the screened compounds occurred regardless of the increased TEER values. This further indicates that the increased TEER (decreased paracellular permeability) is not a restrictive feature for these molecules to cross the monolayer (the in vivo BBB) because of their superior transcellular permeability characteristics.

As mentioned above, barrier function and tight integrity of the BBB are primarily a result of TJs between adjacent BECs. As a consequence of the presence of these TJs, paracellular passive diffusion (between the BECs) of polar compounds is almost impossible [72]. Considering this, the observed in vitro BBB permeation of the study compounds is more likely to occur through transcellular passive diffusion (through the BEC's membranes). Transcellular passive diffusion, also known as the lipophilic pathway, allows small, lipophilic compounds to passively permeate across the BBB through the BECs directly [73]. Given that our data indicates that these selected molecules can cross the in vitro BBB monolayer system via transcellular "lipophilic" pathways, the supporting in silico results together with the preliminary in vitro data confirm that the single compounds and their combinations are BBB-permeable, albeit that they reduced BBB paracellular permeability. In light of this supporting evidence, these compounds and the combination should be assessed further as potential treatments.

Some of this study's limitations include the use of one in silico testing to predict the BBB permeability of the active AChEI compounds and the most potent compound was predicted to be non-BBB permeable leading to it being excluded from further investigation. More than one in silico method (such as machine learning methods) should be used in the future to confirm BBB

predictive results. Even though kinetic results and supporting literature suggest the binding sites of the active compounds, additional molecular docking studies need to be carried out to confirm the exact binding sites and further give an insight as to which substituents and moieties bind to the enzyme and confer to the activity observed. Furthermore, the selected compounds were only screened for one target (AChE enzyme) in the current study, therefore these or other compounds from the same library should further be screened against other AD targets such as Aβ plaques, and be used as multitarget modulators. Bolstered isobologram experiments will afford more clarity on the ratiometric potential of the compounds and the best combinations to take forward for further studies.

In conclusion, although **A51** had the greatest AChEI activity, it was predicted to be in silico BBB-impermeable and was not evaluated further. **C53** (IC_{50}) and the donepezil-**C53** combination with allosteric effect at the lowest doses indicated the potential for further investigation due to the promising acellular and cellular AChEI activity, in silico BBB-permeability, absence of cytotoxicity, and ability to penetrate the in vitro BBB monolayer.

Author Contributions

All authors contributed equally to this work.

Acknowledgments

Ms. Margo Nell for assistance with cell culturing, Prof Paul Steenkamp for the UPLC analysis, Dr. Johan van der Westhuizen for his technical support, and Dr. Shireen Mentor for the training received on in vitro BBB model. Council for Scientific and Industrial Research and Department of Science and Innovation Inter-bursary Scholarship, and the University of Pretoria Postgraduate bursary (grant no: 608664) for financial support.

Conflicts of Interest

The authors declare no conflicts of interest.

Data Availability Statement

The data that support the findings of this study are available on request from the corresponding author.

Declaration of Transparency and Scientific Rigor

This Declaration acknowledges that this paper adheres to the principles for transparent reporting and scientific rigor of preclinical research as stated in the British Journal of Pharmacology guidelines.

References

1. J. Cummings, G. Lee, A. Ritter, and K. Zhong, "Alzheimer's disease drug development pipeline: 2018," *Alzheimer's & Dementia: Translational Research & Clinical Interventions* 4 (2018): 195–214, https://doi.org/10.1016/j.trci.2018.03.009.

2. S. Gauthier, P. Rosa-Neto, J. A. Morais, and C. Webster, *World Alzheimer Report 2021: Journey Through the Diagnosis of Dementia* (London, England: Alzheimer's Disease International, 2021).

3. E. Bomasang-Layno and R. Bronsther, "Diagnosis and Treatment of Alzheimer's Disease: An Update," *Delaware Journal of Public Health* 7, no. 4 (2021): 74–85, https://doi.org/10.32481/djph.2021.09.009.

4. V. Revadigar, R. M. Ghalib, V. Murugaiyah, et al., *Enzyme Inhibitors Involved in the Treatment of Alzheimer's Disease* (Sharjah, United Arab Emirates: Bentham Science Publishers, 2014).

5. K. M. Carvalho, E. Winter, and A. M. de Souza Antunes, "Analysis of Technological Developments in the Treatment of Alzheimer's Disease Through Patent Documents," *Intelligent Information Management* 7, no. 5 (2015): 268–281, https://doi.org/10.4236/iim.2015.75022.

6. A. Kumar, A. Singh, and Ekavali, "A Review on Alzheimer's Disease Pathophysiology and Its Management: An Update," *Pharmacological Reports* 67, no. 2 (2015): 195–203, https://doi.org/10.1016/j.pharep.2014.09.004.

7. M. Bortolami, D. Rocco, A. Messore, et al., "Acetylcholinesterase Inhibitors for the Treatment of Alzheimer's Disease–A Patent Review (2016–Present)," *Expert Opinion on Therapeutic Patents* 31, no. 5 (2021): 399–420, https://doi.org/10.1080/13543776.2021.1874344.

8. S. H. Kim, N. Kandiah, J. L. Hsu, C. Suthisisang, C. Udommongkol, and A. Dash, "Beyond Symptomatic Effects: Potential of Donepezil as a Neuroprotective Agent and Disease Modifier in Alzheimer's Disease," *British Journal of Pharmacology* 174, no. 23 (2017): 4224–4232, https://doi.org/10.1111/BPH.14030.

9. B. Ray, B. Maloney, K. Sambamurti, et al., "Rivastigmine Modifies the α-Secretase Pathway and Potentially Early Alzheimer's Disease," *Translational Psychiatry* 10, no. 1 (2020): 47, https://doi.org/10.1038/S41398-020-0709-X.

10. S. Sharma, "Galantamine Delivery for Alzheimer's Disease. Sustainable Agriculture Reviews 43: Pharmaceutical Technology for Natural Products Delivery," *Fundamentals and Applications* 1 (2020): 131–159, https://doi.org/10.1007/978-3-030-41838-0_5.

11. M. Stazi and O. Wirths, "Chronic Memantine Treatment Ameliorates Behavioral Deficits, Neuron Loss, and Impaired Neurogenesis in a Model of Alzheimer's Disease," *Molecular Neurobiology* 58, no. 1 (2021): 204–216, https://doi.org/10.1007/S12035-020-02120-Z.

12. B. Das, S. Dasgupta, and S. Ray, "Potential Therapeutic Roles of Retinoids for Prevention of Neuroinflammation and Neurodegeneration in Alzheimer's Disease," *Neural Regeneration Research* 14, no. 11 (2019): 1880–1892, https://doi.org/10.4103/1673-5374.259604.

13. E. Karthikeyan, "From Cholinesterase Inhibitors to Glutamate Receptors to Aducanumab: A Therapeutic Review of Alzheimer's Disease," *International Journal of High School Research* 5, no. 5 (2023): 47–52, https://doi.org/10.36838/v5i5.9.

14. I. S. Padd and M. Parmar, *Aducanumab* (Treasure Island (FL): StatPearls Publishing, 2023), https://www.ncbi.nlm.nih.gov/books/NBK573062/.

15. P. K. Singh, E. N. Simões-Pires, Z. L. Chen, et al., "Lecanemab Blocks the Effects of the Aβ/Fibrinogen Complex on Blood Clots and Synapse Toxicity in Organotypic Culture," *Proceedings of the National Academy of Sciences* 121, no. 17 (2024): e2314450121, https://doi.org/10.1073/pnas.2314450121.

16. A. K. Saxena, "The Structural Hybrids of Acetylcholinesterase Inhibitors in the Treatment of Alzheimer's Disease: A Review," *Alzheimer's & Neurodegenerative Diseases* 4 (2019): 1–25, https://doi.org/10.24966/AND-9608/100015.

17. M. Umar, Y. Rehman, S. Ambreen, et al., "Innovative Approaches to Alzheimer's Therapy: Harnessing the Power of Heterocycles, Oxidative Stress Management, and Nanomaterial Drug Delivery System," *Ageing Research Reviews* 10 (2024): 102298, https://doi.org/10.1016/j.arr.2024.102298.

18. P. R. Carlier, E. S. Chow, Y. Han, J. Liu, J. El Yazal, and Y. P. Pang, "Heterodimeric Tacrine-Based Acetylcholinesterase Inhibitors: Investigating Ligand-Peripheral Site Interactions," *Journal of Medicinal Chemistry* 42, no. 20 (1999): 4225–4231, https://doi.org/10.1021/JM990224W.

19. R. J. Obaid, E. U. Mughal, N. Naeem, et al., "Pharmacological Significance of Nitrogen-Containing Five and Six-Membered Heterocyclic Scaffolds as Potent Cholinesterase Inhibitors for Drug Discovery," *Process Biochemistry* 120 (2022): 250–259, https://doi.org/10.1016/j.procbio.2022.06.009.

20. E. Viayna, R. Sabaté, and D. Muñoz-Torrero, "Dual Inhibitors of β-Amyloid Aggregation and Acetylcholinesterase as Multi-Target Anti-Alzheimer Drug Candidates," *Current Topics in Medicinal Chemistry* 13, no. 15 (2013): 1820–1842, https://doi.org/10.2174/15680266113139990139.

21. M. L. Binderup, M. Dalgaard, L. O. Dragsted, et al., *Combined Actions and Interactions of Chemicals in Mixtures: The Toxicological Effects of Exposure to Mixtures of Industrial and Environmental Chemicals* (Soborg, Denmark: Danish Veterinary and Food AdministrationFødevareRapport No.2003:12, 2003), 1–158.

22. A. Kulshreshtha and P. Piplani, "Current Pharmacotherapy and Putative Disease-Modifying Therapy for Alzheimer's Disease," *Neurological Sciences* 37 (2016): 1403–1435, https://doi.org/10.1007/s10072-016-2625-7.

23. Ł. J. Walczak-Nowicka and M. Herbet, "Acetylcholinesterase Inhibitors in the Treatment of Neurodegenerative Diseases and the Role of Acetylcholinesterase in Their Pathogenesis," *International Journal of Molecular Sciences* 22, no. 17 (2021): 9290, https://doi.org/10.3390/IJMS22179290.

24. L. M. Waite, "Treatment for Alzheimer's Disease: Has Anything Changed?," *Australian Prescriber* 38, no. 2 (2015): 60–63, https://doi.org/10.18773/austprescr.2015.018.

25. X. A. Alvarez, R. Cacabelos, C. Sampedro, et al., "Combination Treatment in Alzheimer's Disease: Results of a Randomized, Controlled Trial With Cerebrolysin and Donepezil," *Current Alzheimer Research* 8, no. 5 (2011): 583–591, https://doi.org/10.2174/156720511796391863.

26. V. K. Gribkoff and L. K. Kaczmarek, "The Need for New Approaches in CNS Drug Discovery: Why Drugs Have Failed, and What Can Be Done to Improve Outcomes," *Neuropharmacology* 120 (2017): 11–19, https://doi.org/10.1016/j.neuropharm.2016.03.021.

27. A. Arora, P. Nain, R. Kumari, and J. Kaur, "Major Causes Associated With Clinical Trials Failure and Selective Strategies to Reduce These Consequences: A Review," *Archives of Pharmacy Practice* 12, no. 2 (2021): 45–53, https://doi.org/10.51847/YJQDk2wtgX.

28. L. Berg, C. D. Andersson, E. Artursson, et al., "Targeting Acetylcholinesterase: Identification of Chemical Leads by High Throughput Screening, Structure Determination and Molecular Modeling," *PLoS One* 6 (2011): 26039, https://doi.org/10.1371/journal.pone.0026039.

29. A. F. McKoy, J. Chen, T. Schupbach, and M. H. Hecht, "A Novel Inhibitor of Amyloid β (aβ) Peptide Aggregation: From High Throughput Screening to Efficacy in an Animal Model of Alzheimer Disease," *Journal of Biological Chemistry* 287, no. 46 (2012): 38992–39000, https://doi.org/10.1074/jbc.M112.348037.

30. S. S. Phatak, C. C. Stephan, and C. N. Cavasotto, "High-Throughput and In Silico Screenings in Drug Discovery," *Expert Opinion on Drug Discovery* 4, no. 9 (2009): 947–959, https://doi.org/10.1517/17460440903190961.

31. Ö. S. Aslantürk, *Genotoxicity-A Predictable Risk to Our Actual World* (London, United Kingdom: InTechOpen, 2018).

32. C. W. Fong, "Permeability of the Blood–Brain Barrier: Molecular Mechanism of Transport of Drugs and Physiologically Important Compounds," *Journal of Membrane Biology* 248, no. 4 (2015): 651–669, https://doi.org/10.1007/s00232-015-9778-9.

33. A. Appelt-Menzel, A. Cubukova, K. Günther, et al., "Establishment of a Human Blood-Brain Barrier Co-Culture Model Mimicking the Neurovascular Unit Using Induced Pluri-and Multipotent Stem Cells," *Stem Cell Reports* 8, no. 4 (2017): 894–906, https://doi.org/10.1016/j.stemcr.2017.02.021.

34. L. Peternel, M. Kotnik, A. Preželj, and U. Urleb, "Comparison of 3 Cytotoxicity Screening Assays and Their Application to the Selection of Novel Antibacterial Hits," *SLAS Discovery* 14, no. 2 (2009): 142–150, https://doi.org/10.1177/1087057108329452.

35. C. J. van der Westhuizen, "Discovery of Novel Acetylcholinesterase Inhibitors Using an Integrated Computational and Experimental Approach," (PhD thesis, University of Pretoria: South Africa, 2020).

36. G. L. Ellman, K. D. Courtney, V. Andres, Jr., and R. M. Featherstone, "A New and Rapid Colorimetric Determination of Acetylcholinesterase Activity," *Biochemical Pharmacology* 7, no. 2 (1961): 88–95, https://doi.org/10.1016/0006-2952(61)90145-9.

37. I. M. S. Eldeen, E. E. Elgorashi, and J. Van Staden, "Antibacterial, Anti-Inflammatory, Anti-Cholinesterase and Mutagenic Effects of Extracts Obtained From Some Trees Used in South African Traditional Medicine," *Journal of Ethnopharmacology* 102, no. 3 (2005): 457–464, https://doi.org/10.1016/j.jep.2005.08.049.

38. P. W. Iversen, B. Beck, Y. F. Chen, et al., "HTS Assay Validation," in *Assay Guidance Manual* (Bethesda (MD): Eli Lilly & Company and the National Center for Advancing Translational Sciences, 2012), http://www.ncbi.nlm.nih.gov/books/NBK83783/.

39. A. Daina, O. Michielin, and V. Zoete, "SwissADME: A Free Web Tool to Evaluate Pharmacokinetics, Drug-Likeness and Medicinal Chemistry Friendliness of Small Molecules," *Scientific Reports* 7, no. 1 (2017): 42717, https://doi.org/10.1038/srep42717.

40. A. Daina and V. Zoete, "A Boiled-Egg to Predict Gastrointestinal Absorption and Brain Penetration of Small Molecules," *International Medicinal Chemistry Journal* 11, no. 11 (2016): 1117–1121, https://doi.org/10.1002/cmdc.201600182.

41. D. G. van Greunen, C. J. van der Westhuizen, W. Cordier, et al., "Novel N-Benzylpiperidine Carboxamide Derivatives as Potential Cholinesterase Inhibitors for the Treatment of Alzheimer's Disease," *European Journal of Medicinal Chemistry* 179 (2019): 680–693, https://doi.org/10.1016/j.ejmech.2019.06.088.

42. T. C. Chou and P. Talalay, "Quantitative Analysis of Dose-Effect Relationships: The Combined Effects of Multiple Drugs or Enzyme Inhibitors," *Advances in Enzyme Regulation* 22 (1984): 27–55, https://doi.org/10.1016/0065-2571(84)90007-4.

43. V. Vichai and K. Kirtikara, "Sulforhodamine B Colorimetric Assay for Cytotoxicity Screening," *Nature Protocols* 1, no. 3 (2006): 1112–1116, https://doi.org/10.1038/nprot.2006.179.

44. B. Srinivasan, A. R. Kolli, M. B. Esch, H. E. Abaci, M. L. Shuler, and J. J. Hickman, "TEER Measurement Techniques for In Vitro Barrier Model Systems," *Journal of Laboratory Automation* 20, no. 2 (2015): 107–126, https://doi.org/10.1177/2211068214561025.

45. S. Mentor and D. Fisher, "Exosomes Form Tunneling Nanotubes (TUNTs) in the Blood-Brain Barrier: A Nano-Anatomical Perspective of Barrier Genesis," *Frontiers in Molecular Neuroscience* 15 (2022): 938315, https://doi.org/10.3389/fnmol.2022.938315.

46. K. Ingkaninan, P. Temkitthawon, K. Chuenchom, T. Yuyaem, and W. Thongnoi, "Screening for Acetylcholinesterase Inhibitory Activity in Plants Used in Thai Traditional Rejuvenating and Neurotonic Remedies," *Journal of Ethnopharmacology* 89, no. 2–3 (2003): 261–264, https://doi.org/10.1016/j.jep.2003.08.008.

47. R. H. Ffrench-Constant and B. C. Bonning, "Rapid Microtitre Plate Test Distinguishes Insecticide Resistant Acetylcholinesterase Genotypes in the Mosquitoes *Anopheles albimanus*, An. Nigerrimus and *Culex pipiens*," *Medical and Veterinary Entomology* 3, no. 1 (1989): 9–16, https://doi.org/10.1111/j.1365-2915.1989.tb00468.x.

48. A. Kumar and T. Darreh-Shori, "DMSO: A Mixed-Competitive Inhibitor of Human Acetylcholinesterase," *ACS Chemical Neuroscience* 8, no. 12 (2017): 2618–2625, https://doi.org/10.1021/acschemneuro.7b00344.

49. N. A. Novales and J. P. Schwans, "Comparing the Effects of Organic Cosolvents on Acetylcholinesterase and Butyrylcholinesterase Activity," *Analytical Biochemistry* 654 (2022): 114796, https://doi.org/10.1016/j.ab.2022.114796.

50. A. Martorana, V. Giacalone, R. Bonsignore, et al., "Heterocyclic Scaffolds for the Treatment of Alzheimer's Disease," *Current Pharmaceutical Design* 22, no. 26 (2016): 3971–3995, https://doi.org/10.2174/1381612822666160518141650.

51. S. M. Gupta, A. Behera, N. K. Jain, et al., "Indene-Derived Hydrazides Targeting Acetylcholinesterase Enzyme in Alzheimer's: Design, Synthesis, and Biological Evaluation," *Pharmaceutics* 15, no. 1 (2022): 94, https://doi.org/10.3390/pharmaceutics15010094.

52. A. Deep, R. Kaur Bhatia, R. Kaur, et al., "Imidazo [1, 2-a] Pyridine Scaffold as Prospective Therapeutic Agents," *Current Topics in Medicinal Chemistry* 17, no. 2 (2017): 238–250, https://doi.org/10.2174/1568026616666160530153233.

53. N. Devi, D. Singh, R. K. Rawal, J. Bariwal, and V. Singh, "Medicinal Attributes of Imidazo [1, 2-a] Pyridine Derivatives: An Update," *Current Topics in Medicinal Chemistry* 16, no. 26 (2016): 2963–2994, https://doi.org/10.2174/1568026616666160506145539.

54. A. S. Gurjar, M. N. Darekar, K. Y. Yeong, and L. Ooi, "In Silico Studies, Synthesis and Pharmacological Evaluation to Explore Multi-Targeted Approach for Imidazole Analogues as Potential Cholinesterase Inhibitors With Neuroprotective Role for Alzheimer's Disease," *Bioorganic & Medicinal Chemistry* 26, no. 8 (2018): 1511–1522, https://doi.org/10.1016/j.bmc.2018.01.029.

55. J. Mensch, J. Oyarzabal, C. Mackie, and P. Augustijns, "In Vivo, In Vitro and In Silico Methods for Small Molecule Transfer Across the BBB," *Journal of Pharmaceutical Sciences* 98, no. 12 (2009): 4429–4468, https://doi.org/10.1002/jps.21745.

56. S. Yang, S. Mei, H. Jin, et al., "Identification of Two Immortalized Cell Lines, ECV304 and bEnd3, for In Vitro Permeability Studies of Blood-Brain Barrier," *PLoS One* 12, no. 10 (2017): e0187017, https://doi.org/10.1371/journal.pone.0187017.

57. J. Lehár, A. S. Krueger, W. Avery, et al., "Synergistic Drug Combinations Tend to Improve Therapeutically Relevant Selectivity," *Nature Biotechnology* 27, no. 7 (2009): 659–666, https://doi.org/10.1038/nbt.1549.

58. H. G. Breitinger, *Drug Synergy-Mechanisms and Methods of Analysis* (London, United Kingdom: InTechOpen, 2012).

59. M. P. Mattson and A. Cheng, "Neurohormetic Phytochemicals: Low-Dose Toxins That Induce Adaptive Neuronal Stress Responses," *Trends in Neurosciences* 29, no. 11 (2006): 632–639, https://doi.org/10.1016/j.tins.2006.09.001.

60. M. Pallàs, D. Porquet, A. Vicente, and C. Sanfeliu, "Resveratrol: New Avenues for a Natural Compound in Neuroprotection," *Current Pharmaceutical Design* 19, no. 38 (2013): 6726–6731, https://doi.org/10.2174/1381612811319380005.

61. D. Demirovic and S. I. Rattan, "Curcumin Induces Stress Response and Hormetically Modulates Wound Healing Ability of Human Skin Fibroblasts Undergoing Ageing In Vitro," *Biogerontology* 12, no. 5 (2011): 437–444, https://doi.org/10.1007/s10522-011-9326-7.

62. M. Zaremba-Czogalla, A. Jaromin, K. Sidoryk, A. Zagórska, M. Cybulski, and J. Gubernator, "Evaluation of the In Vitro Cytotoxic Activity of Caffeic Acid Derivatives and Liposomal Formulation Against Pancreatic Cancer Cell Lines," *Materials* 13, no. 24 (2020): 5813, https://doi.org/10.3390/ma13245813.

63. M. Michaelis, N. Hinsch, U. R. Michaelis, et al., "Chemotherapy-Associated Angiogenesis in Neuroblastoma Tumors," *American Journal of Pathology* 180, no. 4 (2012): 1370–1377, https://doi.org/10.1016/j.ajpath.2011.12.011.

64. G. Li, K. Shao, and C. S. Umeshappa, "Recent Progress in Blood-Brain Barrier Transportation Research," in *Brain Targeted Drug Delivery System* (Amsterdam, Netherlands: Elsevier, 2018).

65. R. Richards, H. R. Schwartz, M. E. Honeywell, et al., "Drug Antagonism and Single-Agent Dominance Result From Differences in Death Kinetics," *Nature Chemical Biology* 16, no. 7 (2020): 791–800, https://doi.org/10.1038/s41589-020-0510-4.

66. S. M. Buker, P. A. Boriack-Sjodin, and R. A. Copeland, "Enzyme–Inhibitor Interactions and a Simple, Rapid Method for Determining Inhibition Modality," *Slas Discovery: Advancing Life Sciences R&D* 24, no. 5 (2019): 515–522, https://doi.org/10.1177/2472555219829898.

67. I. G. Dougall and J. Unitt, "Evaluation of the Biological Activity of Compounds," in *Evaluation of the Biological Activity of Compounds: Techniques and Mechanism of Action Studies* (Amsterdam, Netherlands: Elsevier, 2015).

68. E. E. Kasteel, S. M. Nijmeijer, K. Darney, et al., "Acetylcholinesterase Inhibition in Electric Eel and Human Donor Blood: An In Vitro Approach to Investigate Interspecies Differences and Human Variability in Toxicodynamics," *Archives of Toxicology* 94, no. 12 (2020): 4055–4065, https://doi.org/10.1007/s00204-020-02927-8.

69. M. A. Erickson, M. L. Wilson, and W. A. Banks, "In Vitro Modeling of Blood–Brain Barrier and Interface Functions in Neuroimmune Communication," *Fluids and Barriers of the CNS* 17 (2020): 1–16, https://doi.org/10.1186/s12987-020-00187-3.

70. C. Hajal, B. Le Roi, R. D. Kamm, and B. M. Maoz, "Biology and Models of the Blood–Brain Barrier," *Annual Review of Biomedical Engineering* 23 (2021): 359–384, https://doi.org/10.1146/annurev-bioeng-082120-042814.

71. R. C. Brown, A. P. Morris, and R. G. O'Neil, "Tight Junction Protein Expression and Barrier Properties of Immortalized Mouse Brain Microvessel Endothelial Cells," *Brain Research* 1130, no. 1 (2007): 17–30, https://doi.org/10.1016/j.brainres.2006.10.083.

72. B. Gericke, K. Römermann, A. Noack, et al., "A Face-To-Face Comparison of Claudin-5 Transduced Human Brain Endothelial (hCMEC/D3) Cells With Porcine Brain Endothelial Cells as Blood–Brain Barrier Models for Drug Transport Studies," *Fluids and Barriers of the CNS* 17, no. 1 (2020): 1–16, https://doi.org/10.1186/s12987-020-00212-5.

73. S. M. Curley and N. C. Cady, "Biologically-Derived Nanomaterials for Targeted Therapeutic Delivery to the Brain," *Science Progress* 101, no. 3 (2018): 273–292, https://doi.org/10.1016/j.trci.2018.03.009.

Supporting Information

Additional supporting information can be found online in the Supporting Information section.